remote sensing

Article

Characteristics of the Spatio-Temporal Dynamics of Aerosols in Central Asia and Their Influencing Factors

Yongchao Zhou [1,2,3], Xin Gao [2,*], Xiaoyu Meng [4], Jiaqiang Lei [2] and Ümüt Halik [1]

1 College of Ecology and Environment, Xinjiang University, Urumqi 830046, China; zhouyongchao20@mails.ucas.ac.cn (Y.Z.); halik@xju.edu.cn (Ü.H.)
2 State Key Laboratory of Desert and Oasis Ecology, Xinjiang Institute of Ecology and Geography, Chinese Academy of Sciences, Urumqi 830011, China; leijq@ms.xjb.ac.cn
3 University of Chinese Academy of Sciences, Beijing 100049, China
4 Key Research Institute of Yellow River Civilization and Sustainable Development & Collaborative Innovation Center on Yellow River Civilization of Henan Province, Henan University, Kaifeng 475000, China; mengxiaoyu161@mails.ucas.ac.cn
* Correspondence: gaoxin@ms.xjb.ac.cn

Abstract: Aerosols are an important component of the atmospheric system. Long time-series observations for aerosols are essential for examining global climate change and the ecological environment. Based on Google Earth Engine and MODIS MCD19A2 data, we monitored the spatio-temporal dynamic characteristics of the aerosol optical depth (AOD) in Central Asia from 2001 to 2020. The effects of six environmental factors on the AOD distribution were explored using a geographic detector model and analysed in combination with the land-use/land-cover change (LUCC) and desertification in different periods. The results showed that the average multi-year AOD in Central Asia was 0.1442, with insignificant interannual variations. The high-value areas were mainly distributed in the Aral Sea and surrounding areas of the Tarim Basin in Xinjiang, with notable seasonal variations. The evaluation results for the influencing factors showed that the relative humidity and precipitation had a large effect on the spatial distribution of the AOD. The LUCC directly affected contributions to the AOD. Desertification of land provides rich dust sources, which are the main aerosol sources in Central Asia, thus exacerbating dust aerosol pollution. This study investigated the temporal and spatial characteristics and influencing factors of the AOD in Central Asia, providing a theoretical basis for the prevention and control of air pollution.

Keywords: aerosol optical depth; temporal and spatial distribution; geographic detector; Central Asia; desertification

check for updates

Citation: Zhou, Y.; Gao, X.; Meng, X.; Lei, J.; Halik, Ü. Characteristics of the Spatio-Temporal Dynamics of Aerosols in Central Asia and Their Influencing Factors. *Remote Sens.* **2022**, *14*, 2684. https://doi.org/10.3390/rs14112684

Academic Editor: Dimitrios Balis

Received: 30 April 2022
Accepted: 31 May 2022
Published: 3 June 2022

1. Introduction

Aerosols play an important role in the atmospheric radiation balance and in climate change. The relationship between aerosols and climate systems has received increasing attention with our increased understanding of these subjects [1]. The concentration and optical properties of aerosols are the main factors of uncertainty for global climate change and regional air quality predictions [2,3]. The aerosol optical depth (AOD) is an important optical parameter for aerosol concentration estimations, air pollution level evaluations, and aerosol climate effect evaluations. It can measure the extinction ability of aerosols, and partially reflect the vertical concentration of aerosols [4–7]. To evaluate the impact that aerosols have on the climate and ecological environment, we must quantify the impact that the aerosol optical properties have at different temporal and spatial scales [8].

Satellite remote sensing provides technical support for atmospheric environmental research. Since the 1970s, many satellite platforms and sensors have been developed for atmospheric and environmental research [9–12]. The Terra satellite launched by the National Aeronautics and Space Administration (NASA) in 1999 carries Moderate Resolution

Imaging Spectroradiometer (MODIS) and Multi-angle Imaging Spectroradiometer (MISR). Due to its unique multi-angle and multispectral design, it has been providing high-quality AOD data since 24 February 2000, which have been widely used for various studies [13–15] The latest multi-angle atmospheric correction algorithm (MAIAC) AOD data can effectively reflect the spatial pattern of aerosol pollution levels and maintain data reliability under cloudy conditions [16–18]. MAIAC AOD data are more applicable in Central Asia and are better than other AOD data in terms of spatial resolution, which can effectively compensate for the lack of observational data [19].

Dust aerosols account for 40–50% of total global aerosols, and are the largest aerosol source in the world. Global aerosols increase in the spring and summer, during which sandstorm events occur frequently, such that large mineral dust aerosol particles are the main contributor for the increase [20]. Central Asia is located in arid and semi-arid areas; the intensification of desertification has resulted in serious dust storm disasters. Dust from Central Asia and surrounding areas is transported through the westerly wind belt, and has a significant impact on several components, including the mountain cryosphere [21]. Precipitation is scarce and unevenly distributed in Central Asia, and the ecological environment is fragile. Recently, irrigation interception, blind reclamation, and other human activities have resulted in the degradation of lake and vegetation. Particularly, the Aral Sea and Ebinur Lake have rapidly degraded. Dried lake bottoms form part of the saline dust owing to wind erosion, causing serious damage to the surrounding environment and economy [22,23]. Domestic and international studies have investigated aerosols in different regions of Central Asia. For example, Rupakheti et al. [24] analysed variations in the physical, optical, and radiative properties of aerosols during aerosol events in Dushanbe, a typical city in Central Asia. Wang et al. [25] found that the AOD in the Aral Sea area has a notable recent upward trend, where salt dust is the main contributor, whereas the AOD in the Ebinur Lake area has remained basically stable. Hofer et al. [26] measured the vertical optical aerosol characteristics of extreme dust events in Tajikistan using multi-band light detection and ranging (LiDAR) to identify the dust source area using a backward trajectory model. Floutsi et al. [27] found that aerosols in Central Asia have notable spatial variability and seasonal periodicity using MODIS MOD08 data. Micklin [28] found that the aerosol composition and spatial distribution were different owing to the impact of emission sources and the surrounding environment, which changed rapidly with time. Additionally, some scholars have examined the factors affecting the spatial distribution of AOD. Chen et al. [29] found that it is affected by boundary layer height and meteorology. Moreover, not only precipitation and temperature, but also the irrational use of water resources by humans leads to further increases in dust aerosol content [30].

Recently, the degradation of inland lakes and enhanced desertification have led to increasingly serious ecological and environmental problems in Central Asia, which have become a hot topic in global aerosol research [31–33]. Therefore, performing aerosol research in Central Asia is important to prevent and control air pollution and ensure regional ecological security. Based on satellite remote sensing technology, we examined the temporal and spatial dynamic characteristics of the AOD in Central Asia over the last 20 years, and identified the driving elements of AOD. The main objectives were to (1) explore the dynamic distribution characteristics of aerosols in Central Asia, (2) reveal the influencing factors affecting the aerosol distribution in Central Asia, and (3) clarify the relationship between the aerosol distribution characteristics and land use changes in Central Asia. This study can provide a reference for aerosol climate effects at regional and global scales.

2. Study Area

Central Asia is located in the centre of Eurasia and is an important transportation hub linking Asia and Europe (Figure 1). Numerous definitions exist about the extent of Central Asia. In this study, the five Central Asian countries and Xinjiang, China, were considered as the regions of Central Asia [30]. The high mountains on the southeastern edge block the warm and humid airflow from the Indian and the Pacific Ocean. The climate of the region is a typical continental climate with scarce precipitation. Central Asia is far from the ocean; most rivers are inland rivers, and either disappear in the desert or flow into inland lakes. Among them, the Aral Sea, Balkhash Lake, and Ebinur Lake are all inland lakes. Central Asia is an arid and semi-arid region. The Taklimakan Desert, Karakum Desert, Gurbantunggut Desert, and the dry lake bottom of the Aral Sea provide rich sources for global salt and dust aerosol emissions [23]. This has a significant impact on both the ecological environment and on climate change across the vast surrounding areas and globally.

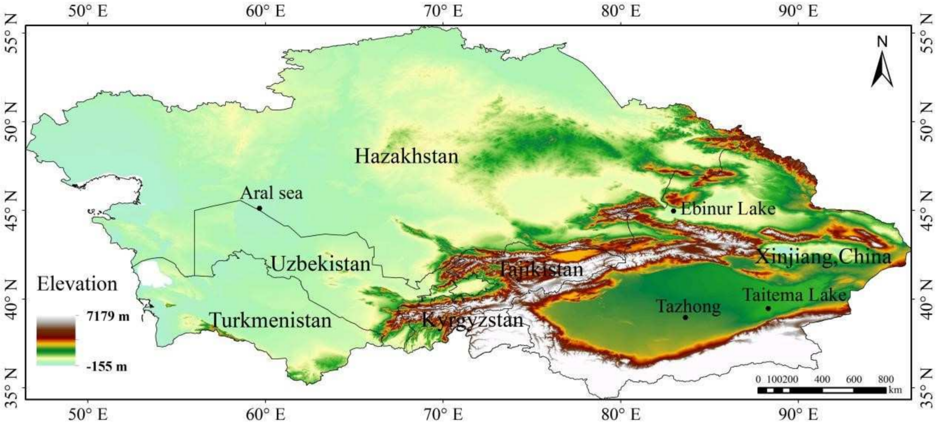

Figure 1. Study area of the five Central Asian countries and Xinjiang, China.

3. Data and Methods

3.1. MODIS AOD

MODIS sensors are widely used in aerosol research owing to their wide spectral range and large coverage area [34,35]. The latest MCD19A2 AOD (https://ladsweb.modaps.eosdis.nasa.gov/search/, accessed on 1 September 2021), a Level 2 product produced using the MAIAC, provides accurate inversions of terrestrial and oceanic aerosol features in subsurface areas with high albedo, such as deserts, plateaus, and other arid areas. Compared with the 10 - and 3 -kilometer resolutions of MOD04 data, its inversion accuracy is high and its spatial resolution is 1 km [17,36]. In this study, daily MCD19A2 AOD data from 2001 to 2020 were used to calculate the mean value of the AOD in different periods using the Google Earth Engine.

MERRA-2 is a new generation of global reanalysis datasets developed based on the Goddard Earth Observing System (GEOS-5.12.4) [37,38]. Since 1980, MERRA-2 has combined aerosol observations from multiple satellites and provides long-term aerosol observation data at a global scale [39]. The spatial resolution is $0.5° \times 0.625°$, and it can distinguish different aerosol types. The AOD comparison between the MERRA-2 and AERONET observations showed that they have a good spatial consistency worldwide [40,41].

3.2. Ground-Based Observation AOD

The ground-based AOD data used in this study were measured by the French CIMEL CE318 series multi-band direct solar radiometer, which is identical to AERONET [42]. The monitoring site was located at the Tazhong Station operated by the China Meteorological Administration (38°58′N, 83°39′E). The meteorological station was located ~200 km into the Taklimakan Desert. The CE-318 instrument can measure aerosols in the 440-, 670-, 870-, and 1020-nanometer bands. The observation period was from March to December 2015. The ground-based AOD data were obtained 30 min before and after the satellite transit time, in order to calculate the AOD value in the 550-nanometer band. The calculation method was as follows:

$$\tau(\lambda) = \tau(\lambda_1) \times (\lambda/\lambda_1)^{-\alpha}, \quad (1)$$

where $\tau(\lambda)$ is the AOD, and α represents the Angstrom wavelength exponent converted by the AOD of different bands, reflecting the proportion of large and small particles in the aerosol component. This parameter was calculated as follows:

$$\alpha = \frac{\ln[\tau(\lambda_1)/\tau(\lambda_2)]}{\ln(\lambda_1/\lambda_2)}, \tag{2}$$

where λ_1 and λ_2 are different wavelengths.

3.3. Environmental Factor Data

Data for six environmental factors in Central Asia from March 2001 to February 2021 were selected, in order to examine the effects that they have on the temporal and spatial distribution of the AOD. The spatial resolution of the temperature, precipitation, and wind speed was $0.1° \times 0.1°$, and the spatial resolution of the relative humidity was $0.25° \times 0.25°$, they are all near-surface data. All data were derived from the ERA5 reanalysis assimilation dataset from the European Centre for Medium-Range Weather Forecasts (https://cds.climate.copernicus.eu/, accessed on 1 October 2021). The surface soil moisture (0–10 cm) data were obtained from the NASA/GLDAS dataset (https://disc.gsfc.nasa.gov/datasets, accessed on 1 October 2021), monthly data with a resolution of $0.1° \times 0.1°$. The NDVI (Normalized Difference Vegetation Index) was obtained from MOD13A1 data (https://ladsweb.modaps.eosdis.nasa.gov/search/, accessed on 1 October 2021), which has a spatial resolution of 500 m.

3.4. Geographic Detector Model

The geographic detector model is based on spatial differentiation theory, which detects the dependent and independent variables after discrete classification at the same spatial scale. If the independent variable has a significant impact on the dependent variable, the spatial distributions of the two variables are somewhat similar [43]. The geographic detector model includes four detectors: risk, factor, ecological, and interaction detectors. The factor detectors can quantitatively describe the extent to which variable X reveals the distribution of variable Y; this correlation can be measured using q statistics. A high q value indicates a high degree of correlation between the two variables; otherwise, it is low. The q value was calculated as follows:

$$q = 1 - \frac{\sum_{H=1}^{L} N_h \sigma_h^2}{N\sigma^2} \tag{3}$$

where σ^2 is the variance of independent variable Y and N is the number of sample points. The superposition of the X and Y variables forms the L layer in Y, which is denoted by H = 1, 2, ..., L. Here, L is the number of classifications after discretization of environmental factors in the data preprocessing stage. Furthermore, N_h denotes the number and variance of samples (pixels) in layer H.

The interaction detector can obtain the explanatory power of the two factors acting together on dependent variable Y. Table 1 classifies their relationships.

Table 1. Effects produced by the interaction between different environmental factors.

Criterion	Interaction Relation
$q(X1 \cap X2) < \mathrm{Min}(q(X1), q(X2))$	Nonlinear weakening
$\mathrm{Min}(q(X1), q(X1)) < q(X1 \cap X1) < \mathrm{Max}(q(X1), q(X1))$	Single-factor nonlinear weakening
$q(X1 \cap X1) > \mathrm{Max}(q(X1), q(X1))$	Two-factor enhancement
$q(X1 \cap X1) = q(X1) + q(X1)$	Independent
$q(X1 \cap X1) > q(X1) + q(X1)$	Nonlinear enhancement

In the data pre-processing stage, the multi-scale discretisation method was used to discretise the environmental factors into six categories. This method can quickly obtain the optimal discretisation results, and optimise the geographic detector model [44].

3.5. LUCC Contribution Calculation

MODIS MCD12Q1 data for 2001, 2007, 2013, and 2019 were used to extract the land-use/land-cover change (LUCC) in Central Asia. There were 17 initial land-cover types in these data based on the International Geosphere-Biosphere Programme, annual data with a resolution of 500 m. Based on the geographical characteristics of Central Asia, land-use types with similar functions were classified into six categories: woodland, grassland, unutilised land (bare land, sandy land with no more than 10% vegetation cover), farmland, construction land, and water.

To quantify the impact that different land cover types have on AOD, the research concept of Chen et al. [45] was cited. First, the ratio between the average AOD corresponding to a specific land-cover type and the average AOD of the entire study area was calculated as follows:

$$dT_i = \frac{\text{mean}(\Delta\text{AOD}_i)}{\text{meanAOD}} \quad (4)$$

where the mean AOD is the average value of the AOD in the entire study area, and mean (ΔAOD) is the average value of the AOD for different land-cover types.

We calculated the contribution of different land-cover types to the AOD as follows:

$$C_i = S_i \times dT_i \quad (5)$$

where S_i is the proportion of each land-cover area. The greater the contribution value of C_i, the greater the contribution of the land-cover type to the AOD.

4. Results and Analysis

4.1. MODIS AOD Data Verification

The AOD of the ground observations was used to validate the MODIS AOD data (Figure 2). The overall trend was consistent, and passed the significance test of $p < 0.05$, with a small standard error of 0.0506, indicating the credible accuracy of MODIS AOD data. Previous studies have used MCD19A2 AOD data, and their results show that these data are accurate [19,46,47]. The inversion principles for satellites and ground-based measured data are different. Ground-based LiDAR is an active remote sensing technique that uses an artificial radiation source to identify the thicknesses of atmospheric particles by receiving a backscattering signal. However, the satellite-based AOD is not free from uncertainties, mostly due to the complex topography/surfaces, cloud contamination, and the models used to retrieve the aerosol, resulting in a bias between the satellite- and ground-measured data [48,49]. Cloud coverage is an important factor in MAIAC AOD misestimation. Furthermore, AOD over- and underestimations were related to the presence of a complex aerosol mixture, especially when dust was mixed with aged anthropogenic aerosol pollution [24].

4.2. AOD Spatio-Temporal Dynamic Characteristics

4.2.1. Multi-Year Average AOD Distribution

The average AOD of all Central Asia from 2001 to 2020 is 0.1442. As shown in Figure 3, the high AOD values were mainly concentrated in the Aral Sea, Ebinur Lake in Xinjiang, and areas surrounding the Tarim Basin. There were significant differences in the AOD among the five Central Asian countries and Xinjiang. The average AOD of the five Central Asian countries from 2001 to 2020 was 0.1246, while that of Xinjiang was 0.1960. The high AOD values in the five Central Asian countries mainly occurred around the Aral Sea, Balkash Lake, and other water bodies. Secondly, most areas of Turkmenistan and Uzbekistan had high AOD values. The low-value areas occurred in the Pamir Plateau area, bordering Tajikistan, and the Kashgar region of Xinjiang. Additionally, the AODs in the Tianshan Mountains and hilly areas of eastern Kazakhstan were relatively low. The spatial distribution of AOD in Xinjiang is affected by the topography of three mountains and two basins, which has notable spatial heterogeneity. The AODs of the Altai Mountains, Kunlun Mountains in the south, and Tianshan, were low. The AOD in the Tarim Basin was generally high, particularly in Ruoqiang, Hotan, and Kashgar. Furthermore, Ebinur Lake, the largest salt-water lake in Xinjiang characterised by loose lake bottom sediments that diffuse under the action of the strong Alashankou wind, had a relatively high AOD in the basin and downwind area.

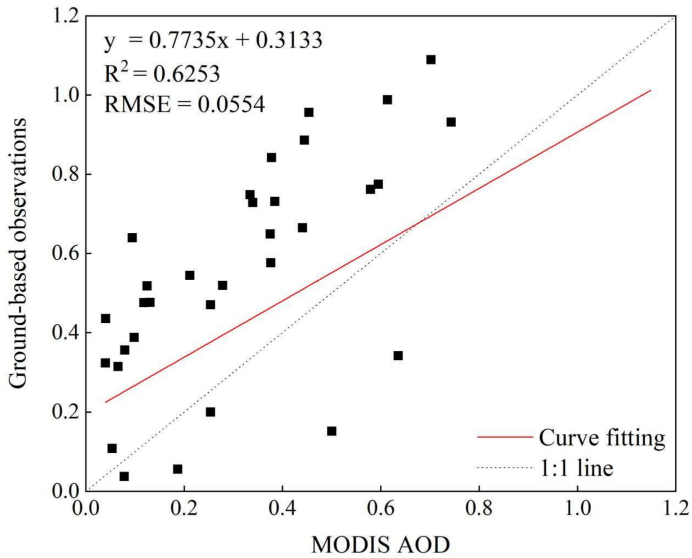

Figure 2. MODIS AOD data verification. The y-axis is the measured value of LiDAR in the Tazhong station, and the x-axis is the MODIS AOD value.

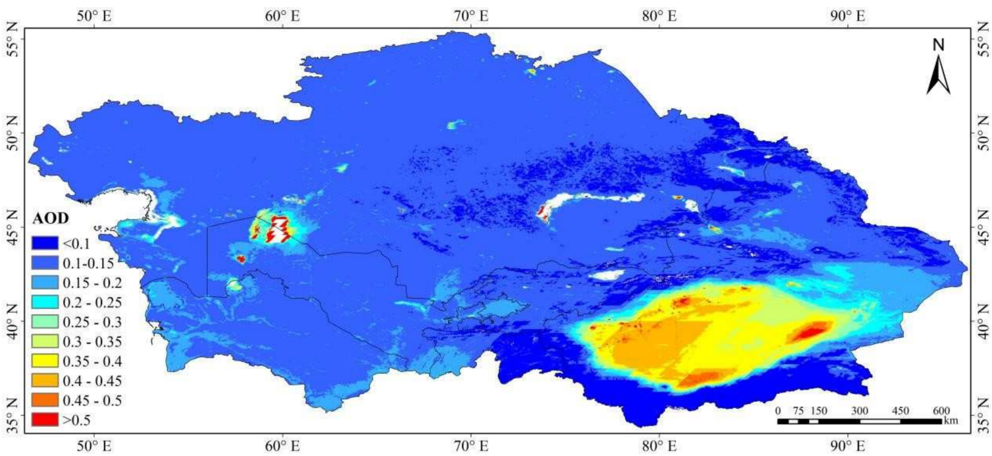

Figure 3. Average AOD distribution in Central Asia from 2001 to 2020.

The distributions of the different aerosol types were analysed using MERRA-2 (Figure 4). The total average multi-year AOD of MERRA-2 was 0.2187, ranging from 0.069 to 0.478. Compared with the MODIS data, the MERRA-2 AOD was larger. The spatial distribution of the two datasets was basically similar in Central Asia, but the spatial resolution of the MERRA-2 data was lower, such that it could not reflect typical areas with high AOD values, e.g., the Aral Sea and Ebinur Lake.

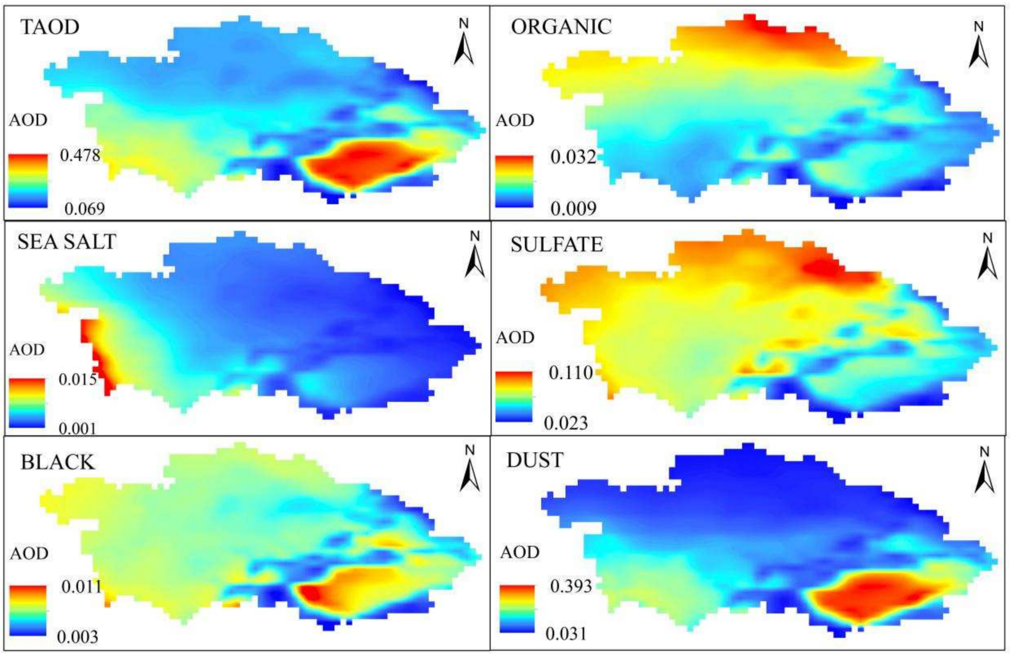

Figure 4. Average distribution of different types of aerosols in MERRA-2 from 2001 to 2020.

Aerosol parameters supported the fact that coarse particles were present in considerable amounts during summer and autumn (influence of natural emissions of dust), whereas fine particles were present during winter (influence of anthropogenic emissions) [15]. Figure 5 shows that dust aerosol is the main aerosol type in Central Asia from 2001 to 2020, up to 82.2%. A high value of 0.393 was observed for the dust AOD in the Taklimakan Desert, followed by the southwest edge of the Tarim Basin. Turkmenistan and Uzbekistan were also areas with a high dust AOD: the Karakum and Kizilkum deserts provide rich dust sources. Except for dust aerosols, the sulphate AOD in the five Central Asian countries was the second highest, but its content was significantly lower than that of the dust AOD. Sulphate aerosols in China were mainly distributed in the east, with a lower sulphate AOD in Xinjiang. The northern slope of the Tianshan Mountains is an area of more concentrated industrial and human activities, such that it had higher levels compared with other locations in Xinjiang. The sulphate AOD in the five Central Asian countries was overall higher than that in Xinjiang; the highest value was observed in northern Kazakhstan. Additionally, the organic carbon, sea salt, and black carbon AOD contents were all low. Central Asia is far from the ocean, and most of these areas are industrially underdeveloped. Only a few areas produce primary and secondary pollutants, such as fuel combustion and industry. The generation of these types of aerosols is closely related to human activities.

4.2.2. Inter-Annual AOD Distribution and Variation

The changes in the spatial distribution of AOD in the five Central Asian countries (Figure 6) was not immediately obvious: the main spatial variation occurred in the Tarim Basin of Xinjiang. The AOD was significantly higher in the western Tarim Basin of Xinjiang in 2006 than in other years. The AOD values of Xinjiang in the past 20 years have generally been higher than those of the five Central Asian countries.

The results of the slope trend analysis (Figure 7) showed that there has been no significant change ($p > 0.05$) in the AOD in most parts of Central Asia over the years. There was a significant increasing trend ($p < 0.01$) in some areas north of the Tianshan Mountains and in a few areas along the southern edge of Xinjiang. The southwestern Aral Sea area and some areas in western Kyrgyzstan showed a significantly increasing trend. The AOD increased relatively ($p < 0.05$) significantly in the western Aral Sea, whereas the southern and eastern areas showed a significantly decreasing trend. The decrease in the

AOD was mainly distributed in northern Kazakhstan, especially in the north-western parts of this region. Figure 8 shows that the average annual AOD in Central Asia has a smaller increasing trend, with minimal inter-annual variations. The lowest AOD (0.1298) occurred in 2005, while the highest AOD (0.1529) occurred in 2006.

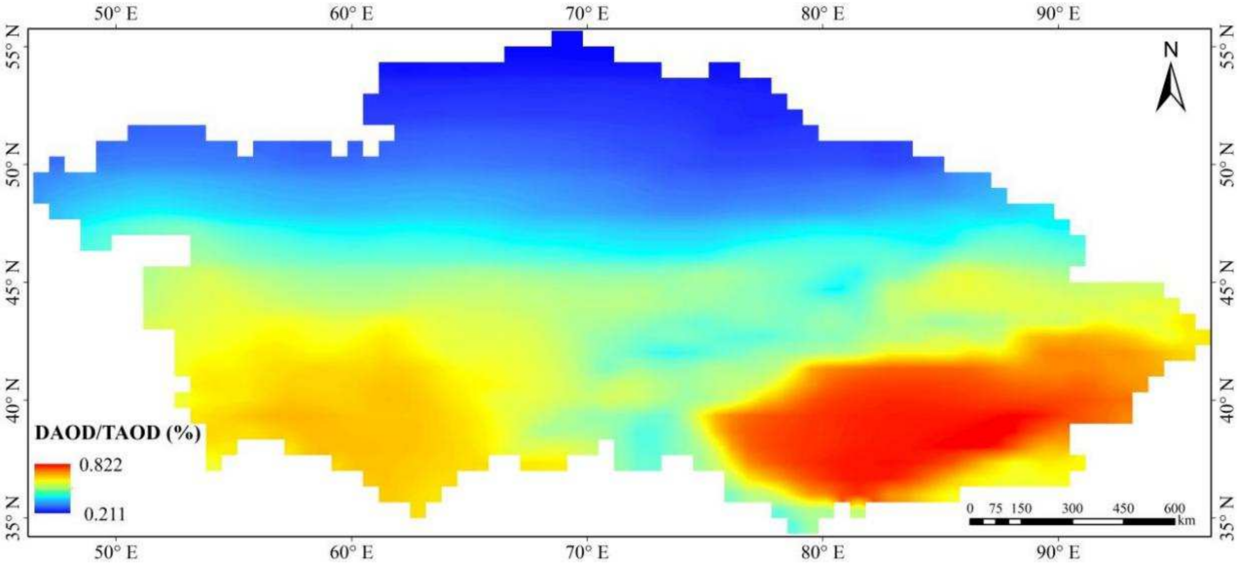

Figure 5. Dust aerosols as a percentage of total aerosols.

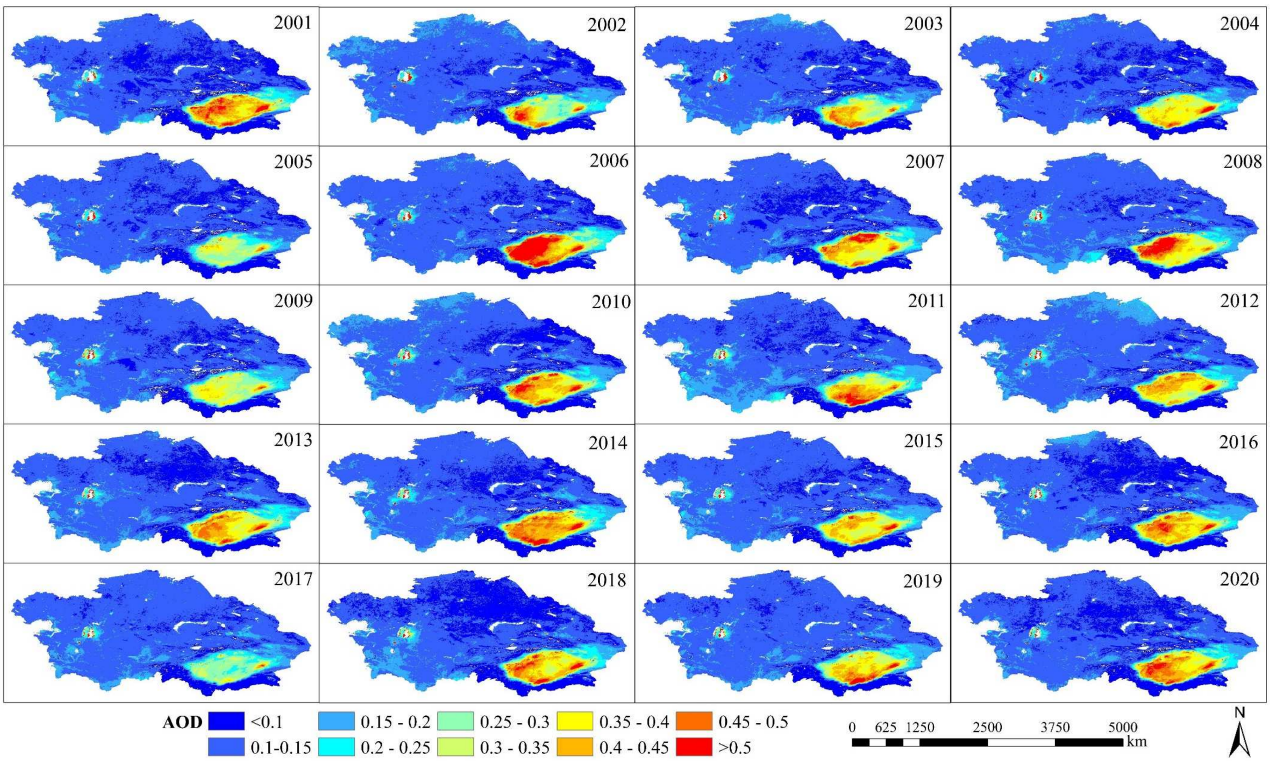

Figure 6. Inter-annual distribution of the AOD in Central Asia.

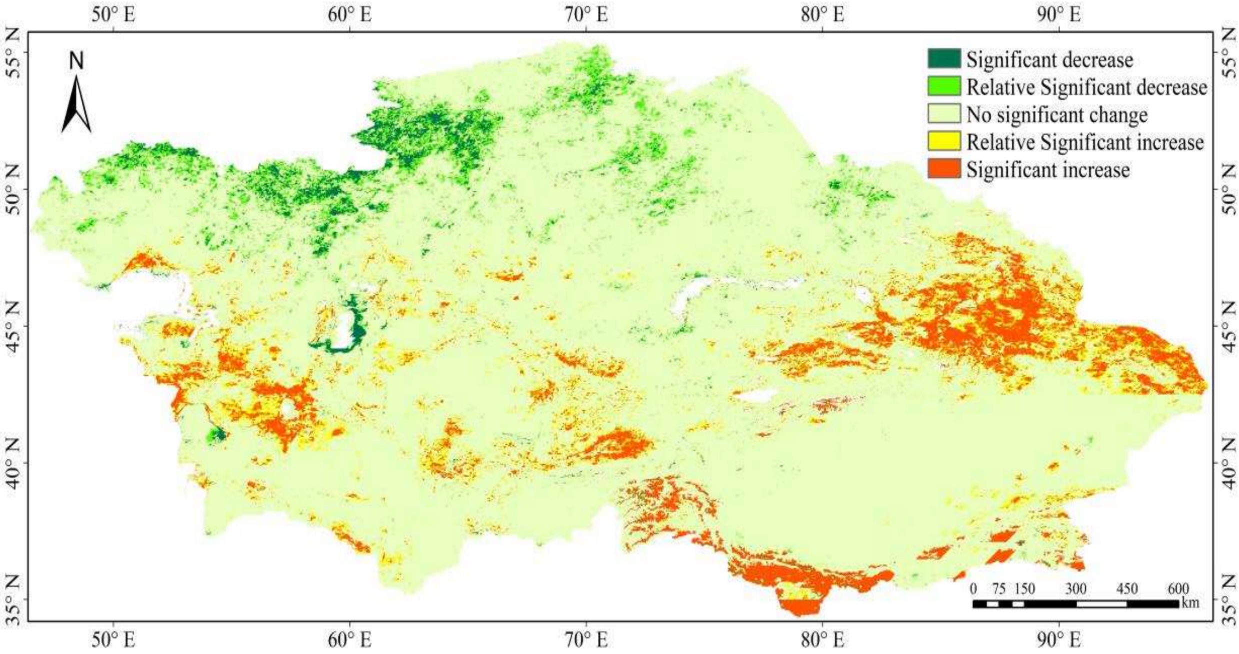

Figure 7. Distribution of the inter-annual variation trends for the AOD in Central Asia from 2001 to 2020.

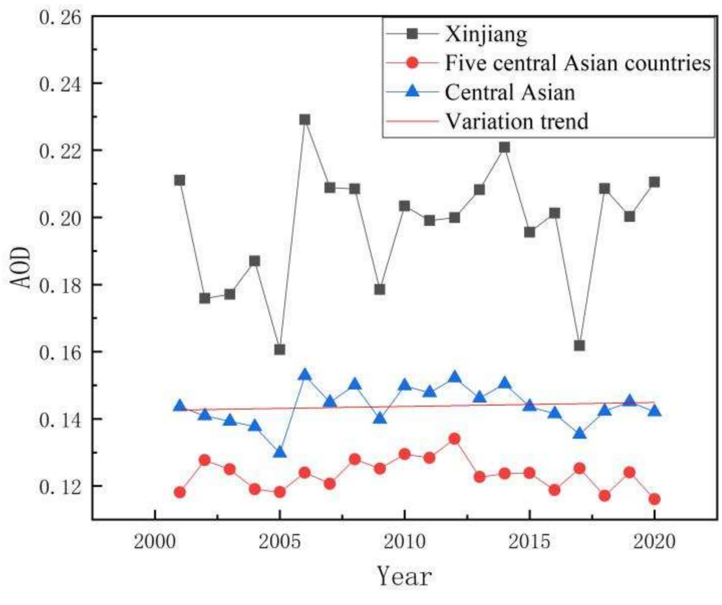

Figure 8. Trends in the AOD across Central Asia.

4.2.3. AOD Distribution and Changes in Different Seasons

Figure 9 shows that the AOD in Central Asia had notable seasonal variation, which is consistent with the results of previous studies [15]. The multi-year AOD had the following order: spring (0.1878) > summer (0.1697) > autumn (0.1243) > winter (0.1165). The rising temperature and melting snow in spring make the soil moisture decrease, and the low precipitation and windy conditions make the loose soil on the surface more prone to dust. It is a season with frequent dusty weather. The AOD of the entire Taklimakan Desert and Aral Sea area, and its surrounding areas, showed high values. In summer, the AOD increased in most areas of Turkmenistan, Uzbekistan, and western and northern Kazakhstan, whereas the AOD decreased significantly in most areas of the northern Taklimakan Desert in Xinjiang. The high value of AOD in the entire study area was found in the southern edge of the Aral Sea and Taklimakan Desert, as well as the city of Ruoqiang in the east. Ruoqiang marks the intersection of the Chelchen and Hotan rivers, and the dry lake of Taitma Lake, Xinjiang, with frequent sand and dust. The AOD in Central Asia decreased significantly during autumn and winter. The peak value of AOD in autumn occurred in the Aral Sea region, followed by the Kashgar region and parts of Ruoqiang in Xinjiang. The lowest AOD occurred in the eastern hills and most of the high-altitude areas in Kazakhstan. The AOD was at a minimum in winter. Snow cover makes it difficult to raise sand on the surface, especially in the Tianshan mountains. The high surface reflectance makes the AOD in the satellite sensor inversion a null value. At this time, a higher AOD value appears in the economic belt on the northern slope of the Tianshan Mountains. This area has a dense population such that the AOD value is significantly higher than that in other places, owing to heating and industrial production emissions in winter. Additionally, the Taklamakan Desert, Karakum Desert, Kizilkum Desert, and Aral Sea had relatively high AOD values.

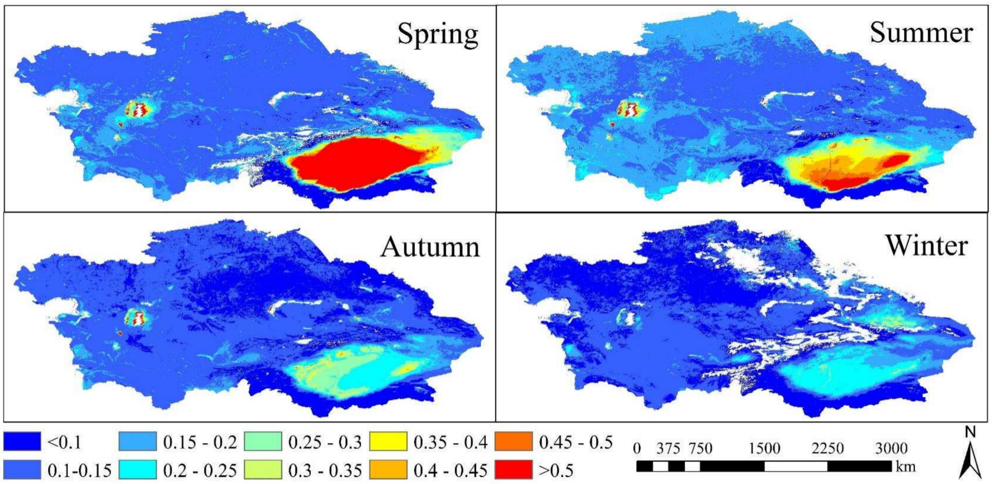

Figure 9. Distribution of the AOD in the four seasons in Central Asia.

The AOD in Central Asia showed a bimodal distribution over the year, however the highest values occurred in different months (Figure 10b). The AOD was higher in March, April, and May in Xinjiang and the entire study area, whereas the AOD was higher in June, July, and August in the five Central Asian countries. The lowest AOD values were observed in November (0.1097).

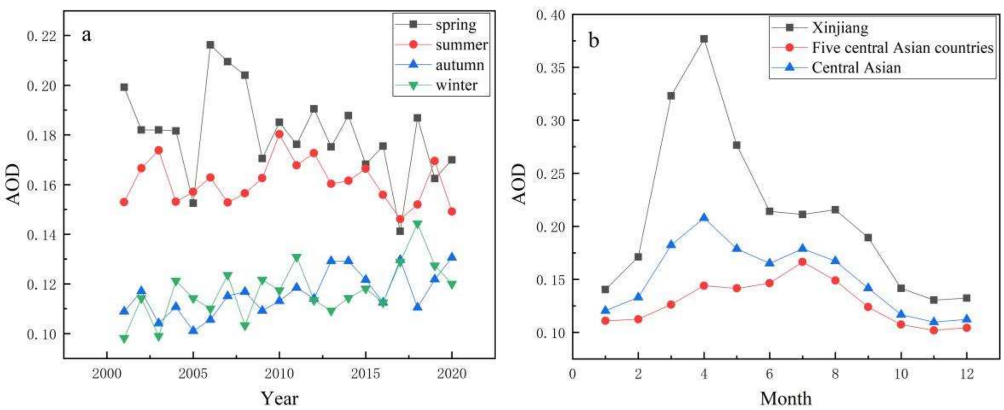

Figure 10. Annual variation of AOD in Central Asia, (**a**) variation of AOD in different seasons; (**b**) Change of AOD in different months.

4.3. AOD Environmental Impact Factors

4.3.1. Single-Factor Effect Analysis

Figure 11 shows the factor detection results. This influence was represented by the q value. The larger the q value, the stronger the influence that the factors have on the spatio-temporal distribution of the AOD. The influence of the environmental factors in descending order was as follows: relative humidity (0.4611) > precipitation (0.4539) > temperature (0.3722) > surface soil moisture (0.2500) > NDVI (0.1850) > wind speed (0.0350). All factors passed the significance test ($p < 0.001$). The relative humidity and precipitation played a dominant role in influencing the aerosol distribution across Central Asia, followed by temperature. Compared with the first three factors, the surface soil moisture, NDVI, and wind speed had a smaller effect on the AOD distribution.

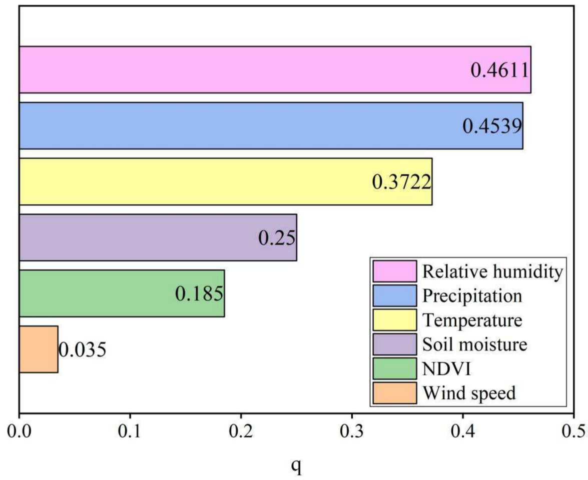

Figure 11. Single-factor detection results.

4.3.2. Two-Factor Interaction Analysis

In the natural environment, a combination of environmental factors affects the temporal and spatial distributions of the AOD. Interaction detection analyses the influence of two environmental factors on the AOD, and further searches for the explanatory ability of the bivariate. Table 2 presents these results. The influence of the two-factor interaction on the spatial distribution of the AOD in Central Asia was greater than that of the single-factor interaction. Factor interaction presents nonlinear enhancement or two-factor enhancement effect, and there are no factors acting independently. The interactions between the NDVI and wind speed, NDVI and temperature, surface soil moisture and wind speed, and temperature and wind speed, were nonlinear enhancements. In other words, the common explanatory power of these factors for the AOD was greater than the sum of the separate explanatory powers of each factor combination, indicating that their joint influence on the aerosol distribution was more notable. Except for the nonlinear enhancement mentioned above, the interactions among the other factors were double-factor enhancement. The q value was the largest for the interaction between the air temperature and relative humidity, reaching 0.6315. This indicated that the combined effect of temperature and relative humidity had the greatest influence on the spatial and temporal distributions of the AOD.

Table 2. Results of the two-factor interaction analysis: influence of two environmental factors together on AOD.

	Relative Humidity	NDVI	Surface Soil Moisture	Precipitation	Temperature	Wind Speed
Relative humidity	0.4611					
NDVI	0.5021	0.1850				
Soil moisture	0.5247	0.3264	0.2500			
Precipitation	0.5229	0.5737	0.5216	0.4539		
Temperature	0.6315	0.5852	0.5829	0.5985	0.3722	
Wind speed	0.4857	0.2363	0.3038	0.4722	0.4119	0.0350

4.3.3. Ranges of Risks Affecting AOD Distribution

Figure 12 shows the results of risk detection in the geographic detector model, reflecting the influence of environmental factors on AOD. The average values of AOD for different ranges of environmental factors can be seen in Figure 12. The risk detection illustrates which environmental factor is more likely to produce AOD in a certain range. The highest AOD values were observed at a relative humidity of 30–34%, the highest risk of an AOD presence in this range. The relative humidity makes atmospheric particles gather in a certain range. Particles settle under the action of gravity with an increase in the relative humidity, accompanied by precipitation, thus decreasing the AOD value. The AOD was the lowest when the relative humidity was between 56 and 81%. As stated by Xi and Sokolik [50], in extremely arid deserts the effect of vegetation and soil moisture are so weak that the dust seasonality is mainly controlled by atmospheric circulation. Thus, the effect of the NDVI on aerosol distribution was not notable; the AOD did not show a regular change with the NDVI. Jiang and Yang [51] found that the oases dramatically reduce the aeolian transport of the sand in the Tarim Basin, but have less effect on the emission of dust particles. The influence of the surface soil moisture on the AOD was relatively small: the lower the soil moisture, the greater the AOD risk. This result was similar to those reported by Han et al. [52], who tested the sensitivity of dust emissions to soil moisture based on the optimal combination of parameterised schemes; analysis showed that the soil moisture had a significant effect on the dust emissions. There was a nonlinear relationship between the two, but sand emissions did not always increase with a decreasing soil moisture content. The influence of precipitation on the aerosol distribution was significant: the greater the precipitation, the smaller the AOD. Precipitation affects dust emission indirectly via changes in soil moisture and vegetation. As a key water supply for desert vegetation, precipitation further inhibits dust emission by reducing soil exposure and increasing surface roughness [50,53] The increase in AOD with increasing temperature is caused by seasonal variations. In Central Asia, the temperature varies significantly with the seasons: the temperature rises in spring and summer, the surface sediment is loose, and the atmospheric particles are easily diffused under airflow transport, thus the AOD is high; in winter, the surface is less likely to blow up sand, and the reduced dust activity makes the AOD smaller. In addition, in areas with relatively stable pollution sources which are affected by meteorological conditions, the higher the temperature, the stronger the atmospheric convective movement, which is conducive to particulate transport. Wind is an important condition for surface sediments. When the surface wind speed reached a certain value, the surface particulate matter jumped, or was even suspended, which increased the concentration of surface atmospheric particulate matter. Therefore, the AOD increases with the increase in wind speed. Xi and Sokolik [54] also illustrated that the decline in dust activity in Central Asia is driven by a decrease in the frequency of strong surface winds. However, wind speed has a smaller effect on AOD compared to other environmental factors in Central Asia. Wind speed enhances near-surface sand activity, but dust aerosols can even be suspended in the atmosphere at a height of several kilometers. AOD can be explained not only by the magnitude of wind speed, it is also subject to a combination of other factors.

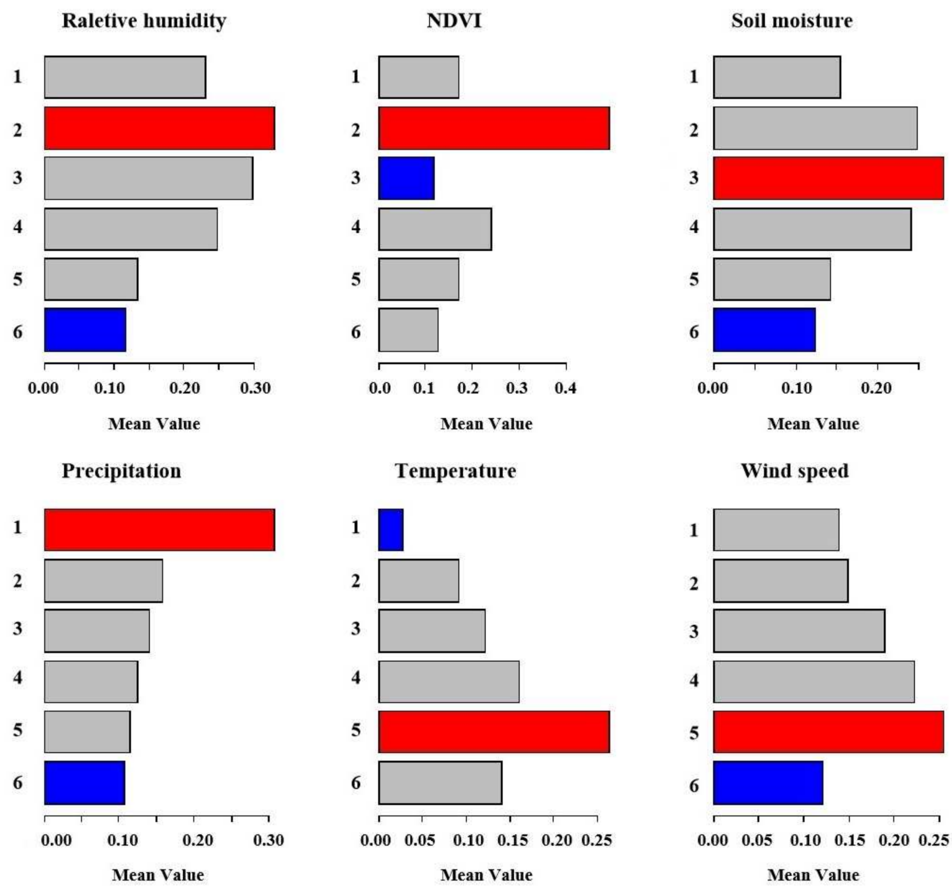

Figure 12. Risk detection results: the *x*-axis is the mean value of AOD under the influence of different factors; the *y*-axis shows the different ranges of factors, gradually increasing from 1 to 6. Red and blue colors indicate the highest and lowest AOD values in this range, respectively.

5. Discussion

5.1. Contribution of LUCC to AOD

Current studies lack an exploration of the relationship between LUCC and aerosols in Central Asia. Regional climate change and interactions with extensive land-cover/land-use changes have resulted in great changes in dryland landscape, and large impacts on atmospheric dust aerosols [54]. The interplay between natural processes and human land use has long been known as a key player in the dryland landscape dynamics and dust variability in Central Asia [55]. Human activities can lead to changes in the underlying surface. On the one hand, various land types and landscape patterns directly affect the AOD. On the other hand, changes in surface structure cause changes in the local climate, which affect aerosol migration and transformation [56]. Improper land use can exacerbate the dryland vulnerability to wind erosion, and lead to increased anthropogenic contribution to the global dust burden [57]. LUCC data for Central Asia in 2001, 2007, 2013, and 2019 were selected, in order to extract the area proportions of different land types. The results (Figure 13) showed that grassland areas in Central Asia accounted for the largest proportion (>50%). The area proportions were as follows: grassland > unutilised land > farmland > water body > woodland > construction land. The area comparison of land types in the four periods showed that the area of unutilised land and farmland has decreased, while there has been an increase in four other land types. Significant changes have occurred in woodland and farmland areas. In 2019, woodland has increased by a factor of one and farmland decreased by half, as compared with 2001. The research concept of Chen et al. [45] was cited to calculate the contribution of land use to AOD. The area share of different land types directly affects their contributions to the AOD distribution. The larger the proportion of a certain land use type, the greater its contribution value (C_i) to the AOD. The contribution of different land types to the AOD in Central Asia was as follows: grassland > unutilised land > farmland > water > woodland > construction land. Human activity mainly affects the LUCC, which also indirectly explains the impact that human activity has on the AOD.

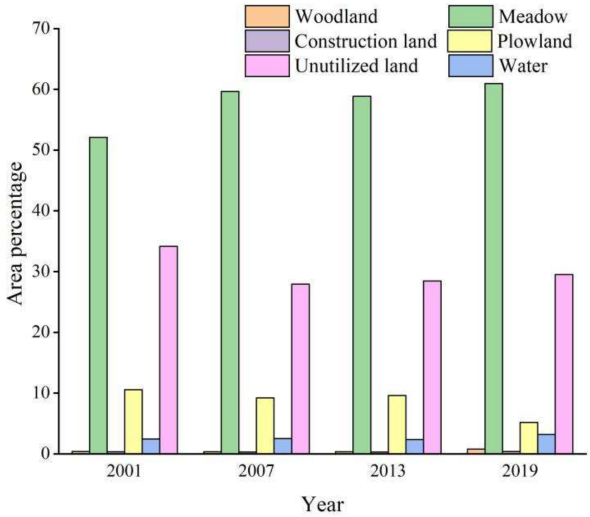

Figure 13. Areas of different land use types in different years in Central Asia.

For a single land type, when the difference between the AOD of the entire study area and the AOD corresponding to different land types is > 1, this indicates that the AOD of the particular land type is large. If the difference is < 1, the AOD of this land type is low. As listed in Table 3, water bodies and unutilised land had the highest AOD, followed by construction land and farmland; grassland and woodland land had lower AOD values. The ecosystem of Central Asia is extremely fragile, rendering it sensitive to climate change and human activity. Shrinking lakes in the Aral Sea region have caused bottom exposure across large areas of lakes; dry lake bottoms provide a rich source of sand and salt dust. The quantity of sand and salt dust increases with further expansion of the desertification area, rendering it as a high-value AOD area in Central Asia. Intensive irrigation in the SYR and Amu Darya rivers accelerates the desertification process of lake bottoms and of the surrounding cultivated land [28]. Owing to dry lake bottoms, sand and salt particles can form disastrous weather events under the action of the northwest wind [58]. Additionally, the increased mineralisation of river water accelerates the salinisation of irrigated land, forcing a reduction in or even inhibition of agricultural production in certain places. Eighty percent of the land across the northern part of the lake is, to varying degrees, endangered by desertification.

Table 3. Difference and contribution of the average AOD of different land use types.

	2001		2007		2013		2019		AOD
	dT_i	C_i	dT_i	C_i	dT_i	C_i	dT_i	C_i	
Woodland	0.73	0.0028	0.74	0.0025	0.67	0.0023	0.76	0.0060	0.1046
Grassland	0.77	0.4029	0.81	0.4851	0.80	0.4699	0.84	0.5133	0.1169
Construction land	0.96	0.0032	1.00	0.0032	1.04	0.0033	1.01	0.0037	0.1457
Farmland	0.95	0.1002	0.98	0.0907	1.01	0.096	1.01	0.0524	0.1431
Water	1.05	0.3000	1.19	0.0300	0.92	0.0219	1.34	0.0425	0.1627
Unutilised land	1.36	0.4663	1.40	0.3911	1.43	0.4058	1.31	0.3876	0.1994

Similar to the Aral Sea, Ebinur Lake in Xinjiang is characterised by heavily exposed dry lake bottoms owing to natural and anthropogenic influences [59,60]. The strong Alashankou wind in the northwest affects the aerosols in the basin. The high AOD of the basin itself has a significant impact on the downwind direction. Additionally, dust sources in the Tarim

Basin are mainly derived from the desert, sandy land, and bare land on the northwest edge of the Taklimakan Desert, as well as the vast oasis desert ecotone [61]. These potential dust source areas contribute significantly to the AOD.

5.2. Impact of Desertification on AOD

Desertification is one of the most prominent ecological and environmental problems in arid and semi-arid regions. Desertification causes hazards such as reduced agricultural and livestock production, frequent wind and sand disasters, and a decrease in the value of ecosystem services in dryland. Desertification intensifies wind erosion and dust emission sources while degrading the air quality in the downwind direction [62]. Using the method proposed in Meng et al. [63], the degree of land desertification in Xinjiang was divided into four classes: light, moderate, severe, and extremely severe desertification. The area proportion of the desertification degree in the four periods was extracted, as listed in Table 4. As can be seen from Figure 14, desertification is widespread in Xinjiang; only a few areas are non-desertified. Non-desertification land is mainly distributed in the Altai Mountains, Tianshan Mountains, the northwest edge of the Tarim Basin, and most areas of the Yili River Valley. Compared with 2001, the area of extremely severe desertification decreased during the three other years. During these years, there was a slight increase in the proportion of non-desertification land, which was more notable in the Tianshan Mountains and the northwestern edge of the Tarim Basin. The proportion of light and severe desertification areas was the smallest, with no significant changes. Generally, light and severe desertification land is adjacent to non-desertified land, and is distributed sporadically. The proportion of severe desertification land increased, and was distributed in the Junggar Basin and along the southern edge of the Tarim Basin. The decreasing area of extremely severe desertification was identical to the increasing area of severe desertification, indicating that extremely severe desertification is transferred to severe desertification.

Table 4. Proportion of the desertification degree area in Xinjiang in different years (%).

	Non-Desertification	Light Desertification	Moderate Desertification	Severe Desertification	Extremely Severe Desertification
2001	8.52	2.57	3.04	12.60	73.27
2007	9.37	2.65	3.12	13.93	70.93
2013	12.16	2.77	3.36	19.38	62.33
2020	11.89	2.74	3.37	18.56	63.44

Overall, there was a decreasing degree in desertification in Xinjiang. Consistent with the trend observed in this study, Li et al. [64] showed that the desertification situation in Xinjiang has improved overall, in which the desertification in northern Xinjiang has improved significantly, whereas improvements in southern and eastern Xinjiang have been slightly worse. However, compared with the four average annual AOD values in Xinjiang, there was no significant difference. The reduction in the desertification of a few areas had no notable impact on the AOD. Xinjiang is located in the centre of Asia, far from the ocean, such that humid water vapour cannot easily reach this area. The Taklimakan and Gurbantunggut deserts occupy more than half of Xinjiang. Precipitation is low and evaporation is high throughout the year: the average annual precipitation in the Tarim Basin is < 100 mm. Sparse vegetation on the lower bedding surface and low soil moisture provide conditions for extremely serious land desertification. Xinjiang is a key area for land salinisation in China. Desert, sand, dry land, bare soil, and dry rivers with the surrounding salinised land are the main types of dust sources. Human activity diverts water from the river into the oasis, such that the area of the oasis has gradually expanded, with continual improvements to the internal environment. There has been a continual decrease in the water volume and groundwater levels in the middle and lower reaches of these rivers, as well as a decline in vegetation, exacerbating desertification. Desertification alerts in Xinjiang were mainly distributed in the lower part of the oasis, around the river channel, and at the river terminus [64]. For example, Ebinur Lake is shrinking and the lakeside vegetation has declined, as a result of a decrease in the groundwater level. Since the middle of the 20th century, owing to the influence of both climate change and human activities, the bottom of Ebinur Lake has been exposed, the sand source has expanded, and the trend of land desertification in the basin has become increasingly intense. Similar situations occur adjacent to other dry lakes, such as Lop Nor, Taitma Lake, and Manas Lake. As a result of incomplete planning during development and utilisation, serious desertification has occurred in the Chelchen and Hotan river basins, as well as in the Tarim Basin and Manas River in the Junggar Basin [60]. Chi [65] examined two dust events in the spring in southern Xinjiang, based on MODIS and Landsat. Yuli County is located along the northeast edge of the Tarim Basin, and Ruqiang County is located along the southeast edge of the Taklamakan Desert. These two counties have a high degree of land salinisation, resulting in more serious land desertification. This shows that sandy and salinised land becomes the main dust source type in the region, affecting the temporal and spatial distributions of the AOD.

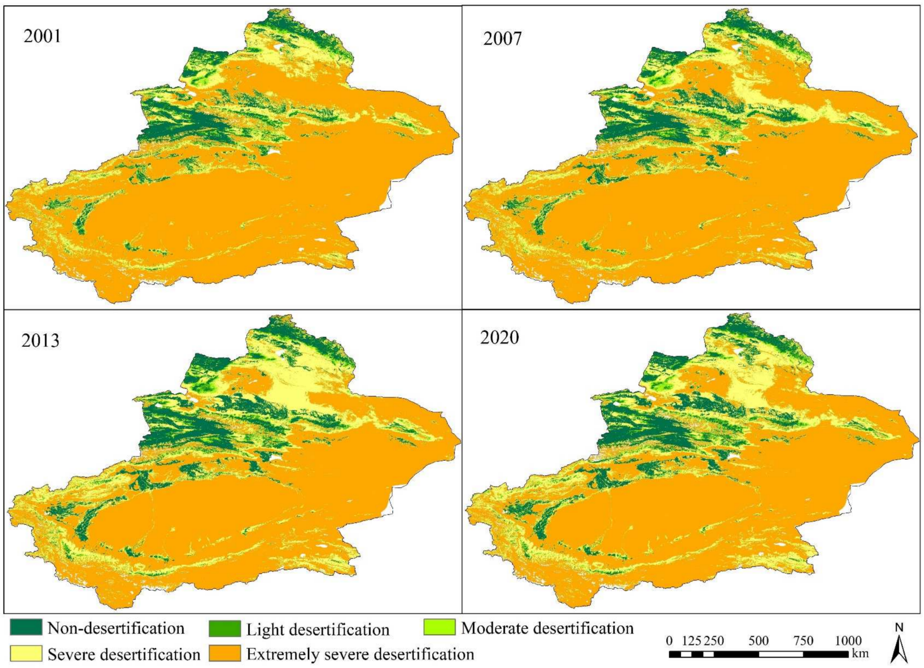

Figure 14. Desertification degree of Xinjiang in different years.

Desertification caused by the drying of Lake Urmia in Iran has led to dust storms in the lake basin, resulting in a significant increase in aerosol pollution [66]. Land degradation and desertification have increased the frequency of dust outbreaks in Hor al-Azim, Iraq, and some arid areas, which is the main factor affecting the aerosol concentration in western Iran [67]. Many studies have shown that desertification land provides rich material sources for dust aerosols, i.e., desertification promotes aerosol production. Central Asia is the largest arid area on Earth. Deserts, semi-deserts, and grasslands occupy most of this region. Desertification has therefore attracted significant attention, especially with respect to salt dust in the Aral Sea. Chen et al. [68] showed that the desertification area of the five Central Asian countries had a northward expansion trend from 2000 to 2015. Turkmenistan, Uzbekistan, and south-central Kazakhstan are characterised by plains, lowlands, and deserts, with a sparse river network density and high levels of desertification. In this study, the desertification degree of the five Central Asian countries was consistent with the spatial distribution of AOD. This indicates that the higher the degree of desertification, the greater the AOD. Therefore, desertification in Central Asia must be a priority. Effective water resource management and rational land use are highly important to the regional atmospheric environment and ecological security.6. Conclusions

Characterised by an arid climate and widespread deserts, Central Asia is one of the important sources of global dust aerosols. Based on MODIS AOD data, we examined the temporal and spatial dynamic characteristics of the AOD in Central Asia from 2001 to 2020. Six environmental factors (i.e., the relative humidity, temperature, precipitation, surface soil humidity, wind speed, and NDVI) were detected using a geographic detector model to analyse the influence on the AOD. The effects of the LUCC and desertification on the AOD distribution were discussed. The following conclusions can be drawn:

(1) The temporal and spatial distributions of the AOD in Central Asia were uneven. The average AOD in Xinjiang was significantly higher than that in the five Central Asian countries. The high-value areas were mainly located in the Aral Sea and Ebinur Lake in Xinjiang, and the peripheral areas of the Tarim Basin. The low-value area was in the Pamir Plateau, an area bordering Tajikistan and Xinjiang. Additionally, the AOD of the mountains and hills in eastern Kazakhstan was relatively low. The inter-annual variation in the AOD was not significant, but there were notable seasonal differences. The AOD value was the highest in the spring and lowest in the winter. Dust aerosols were the main aerosol types in Central Asia.
(2) The results showed that the relative humidity and precipitation had a significant influence on the distribution of the AOD in Central Asia. There was no significant difference between them. The combined action of the temperature and relative humidity had the greatest influence on the temporal and spatials distribution of the AOD, which was a two-factor enhancement.
(3) The LUCC directly affects the temporal and spatial distributions of the AOD. The contribution of different land types to the AOD in Central Asia increased with an increase in the area: grassland > unutilised land > cultivated land > water body > forest land > construction land. The AODs of waterbodies and unutilised land were the highest, whereas that of forest land was the lowest.
(4) Land desertification in Xinjiang is a serious problem: there has been a recent decrease in the degree of desertification. The extremely severe desertification area was consistent with the high-value AOD area. The degree of desertification is serious in inland lakes, such as Ebinur Lake, the middle and lower reaches of oasis rivers, and the desert oasis transition zone, which is an important aerosol source. Desertification has increased the concentration of dust aerosols. Therefore, Central Asia should focus on desertification and rationally utilise land and water resources to effectively control aerosol pollution.

Author Contributions: Y.Z.: data curation, methodology, writing—original draft. X.G.: conceptualization, methodology, writing—review and editing, project administration. J.L.: supervision, visualization. X.M.: data curation, methodology, software. Ü.H.: review, supervision. All authors have read and agreed to the published version of the manuscript.

Funding: This work was supported by the Strategic Priority Research Program of the Chinese Academy of Sciences (No. XDA20030102) and the High-level Talent Cultivation Project from the Xinjiang Institute of Ecology and Geography, Chinese Academy of Sciences (No. E0500201).

Conflicts of Interest: The authors declare that they have no known competing financial interest or personal relationships that could have influenced the work reported in this paper.

Abbreviations

AOD, aerosol optical depth; NASA, National Aeronautics and Space Administration; MODIS, Moderate Resolution Imaging Spectroradiometer; MISR, Multi-angle Imaging Spectroradiometer; MAIAC, multi-angle atmospheric correction algorithm; GEOS, Goddard Earth Observing System; LUCC, land-use/land-cover change.

References

1. Intergovernmental Panel on Climate Change (IPCC). *The Physical Science Basis: Working Group I Contribution to the Fifth Assessment Report of the Intergovernmental Panel on Climate Change*; Cambridge University Press: Cambridge, UK; New York, NY, USA, 2013; Available online: http://www.climatechange2013.org (accessed on 1 October 2021).
2. Che, H.; Zhang, X.; Alfraro, S.; Chatenet, B.; Gomes, L.; Zhao, J. Aerosol optical properties and its radiative forcing over Yulin, China in 2001 and 2002. *Adv. Atmos. Sci.* **2009**, *26*, 564–576. [CrossRef]
3. Hansen, J.; Sato, M.; Ruedy, R.; Lacis, A.; Oinas, V. Global warming in the twenty-first century: An alternative scenario. *Proc. Natl. Acad. Sci. USA* **2000**, *97*, 9875–9880. [CrossRef] [PubMed]
4. He, J.; Zha, Y.; Zhang, J.; Gao, J. Aerosol indices derived from MODIS data for indicating aerosol-induced air pollution. *Remote Sens.* **2014**, *6*, 1587–1604. [CrossRef]
5. Hu, X.-M.; Klein, P.M.; Xue, M.; Zhang, F.; Doughty, D.C.; Forkel, R.; Joseph, E.; Fuentes, J.D. Impact of the vertical mixing induced by low-level jets on boundary layer ozone concentration. *Atmos. Environ.* **2013**, *70*, 123–130. [CrossRef]
6. Lohmann, U. Aerosol effects on clouds and climate. *Space Sci. Rev.* **2007**, *125*, 129–137. [CrossRef]
7. Peng, Z.; Zhang, M.; Kou, X.; Tian, X.; Ma, X. A regional carbon data assimilation system and its preliminary evaluation in East Asia. *Atmos. Chem. Phys.* **2015**, *15*, 1087–1104. [CrossRef]
8. Koffi, B.; Schulz, M.; Bréon, F.M.; Dentener, F.; Steensen, B.M.; Griesfeller, J.; Winker, D.; Balkanski, Y.; Bauer, S.E.; Bellouin, N.; et al. Evaluation of the aerosol vertical distribution in global aerosol models through comparison against CALIOP measurements: AeroCom phase II results. *J. Geophys. Res. Atmos.* **2016**, *121*, 7254–7283. [CrossRef]
9. Hsu, N.C.; Herman, J.R.; Torres, O.; Holben, B.N.; Tanre, D.; Eck, T.F.; Smirnov, A.; Chatenet, B.; Lavenu, F. Comparisons of the TOMS aerosol index with Sun-photometer aerosol optical thickness: Results and applications. *J. Geophys. Res. Atmos.* **1999**, *104*, 6269–6279. [CrossRef]
10. Hsu, N.C.; Lee, J.; Sayer, A.M.; Carletta, N.; Chen, S.-H.; Tucker, C.J.; Holben, B.N.; Tsay, S.-C. Retrieving near-global aerosol loading over land and ocean from AVHRR. *J. Geophys. Res. Atmos.* **2017**, *122*, 9968–9989. [CrossRef]
11. Sayer, A.M.; Hsu, N.C.; Bettenhausen, C.; Jeong, M.-J.; Holben, B.N.; Zhang, J. Global and regional evaluation of over-land spectral aerosol optical depth retrievals from SeaWiFS. *Atmos. Meas. Tech.* **2012**, *5*, 1761–1778. [CrossRef]
12. Wang, Q.; Li, Z.; Guo, J.; Zhao, C.; Cribb, M. The climate impact of aerosols on the lightning flash rate: Is it detectable from long-term measurements? *Atmos. Chem. Phys.* **2018**, *18*, 12797–12816. [CrossRef]
13. Garay, M.J.; Witek, M.L.; Kahn, R.A.; Seidel, F.C.; Limbacher, J.A.; Bull, M.A.; Diner, D.J.; Hansen, E.G.; Kalashnikova, O.V.; Lee, H.; et al. Introducing the 4.4 km spatial resolution Multi-Angle Imaging SpectroRadiometer (MISR) aerosol product. *Atmos. Meas. Tech.* **2020**, *13*, 593–628. [CrossRef]
14. Sayer, A.M.; Hsu, N.C.; Lee, J.; Kim, W.V.; Dutcher, S.T. Validation, Stability, and Consistency of MODIS Collection 6. 1 and VIIRS Version 1 Deep blue aerosol data over land. *J. Geophys. Res. Atmos.* **2019**, *124*, 4658–4688. [CrossRef]
15. Rupakheti, D.; Kang, S.; Bilal, M.; Gong, J.; Xia, X.; Cong, Z. Aerosol optical depth climatology over Central Asian countries based on Aqua-MODIS Collection 6.1 data: Aerosol variations and sources. *Atmos. Environ.* **2019**, *207*, 205–214. [CrossRef]
16. Chudnovsky, A.; Tang, C.; Lyapustin, A.; Wang, Y.; Schwartz, J.; Koutrakis, P. A critical assessment of high-resolution aerosol optical depth retrievals for fine particulate matter predictions. *Atmos. Chem. Phys.* **2013**, *13*, 10907–10917. [CrossRef]
17. Chudnovsky, A.A.; Kostinski, A.; Lyapustin, A.; Koutrakis, P. Spatial scales of pollution from variable resolution satellite imaging. *Environ. Pollut.* **2013**, *172*, 131–138. [CrossRef]
18. Rogozovsky, I.; Ansmann, A.; Althausen, D.; Heese, B.; Engelmann, R.; Hofer, J.; Baars, H.; Schechner, Y.; Lyapustin, A.; Chudnovsky, A. Impact of aerosol layering, complex aerosol mixing, and cloud coverage on high-resolution MAIAC aerosol optical depth measurements: Fusion of lidar, AERONET, satellite, and ground-based measurements. *Atmos. Environ.* **2021**, *247*, 118163. [CrossRef]
19. Chen, X.; Ding, J.; Liu, J.; Wang, J.; Ge, X.; Wang, R.; Zuo, H. Validation and comparison of high-resolution MAIAC aerosol products over Central Asia. *Atmos. Environ.* **2021**, *251*, 118273. [CrossRef]
20. Gui, K.; Che, H.; Zheng, Y.; Wang, Y.; Zhang, L.; Zhao, H.; Li, L.; Zhong, J.; Yao, W.; Zhang, X. Seasonal variability and trends in global type-segregated aerosol optical depth as revealed by MISR satellite observations. *Sci. Total Environ.* **2021**, *787*, 147543. [CrossRef]
21. Kang, S.; Zhang, Q.; Qian, Y.; Ji, Z.; Li, C.; Cong, Z.; Zhang, Y.; Guo, J.; Du, W.; Huang, J.; et al. Linking atmospheric pollution to cryospheric change in the Third Pole region: Current progress and future prospects. *Natl Sci. Rev.* **2019**, *6*, 796–809. [CrossRef]
22. Shen, H.; Abuduwaili, J.; Ma, L.; Samat, A. Remote sensing-based land surface change identification and prediction in the Aral Sea bed, Central Asia. *Int. J. Environ. Sci. Technol.* **2019**, *16*, 2031–2046. [CrossRef]
23. Gaybullaev, B.; Chen, S.-C.; Kuo, Y.-M. Large-scale desiccation of the Aral Sea due to over-exploitation after 1960. *J. Mt. Sci.* **2012**, *9*, 538–546. [CrossRef]
24. Rupakheti, D.; Rupakheti, M.; Yin, X.; Hofer, J.; Rai, M.; Hu, Y.; Abdullaev, S.F.; Kang, S. Modifications in aerosol physical, optical and radiative properties during heavy aerosol events over Dushanbe, Central Asia. *Geosci. Front.* **2021**, *12*, 101251. [CrossRef]
25. Wang, T.; Chen, Y.; Gan, Z.; Han, Y.; Li, J.; Huang, J. Assessment of dominating aerosol properties and their long-term trend in the Pan-Third Pole region: A study with 10-year multi-sensor measurements. *Atmos. Environ.* **2020**, *239*, 117738. [CrossRef]

26. Hofer, J.; Ansmann, A.; Althausen, D.; Engelmann, R.; Baars, H.; Abdullaev, S.F.; Makhmudov, A.N. Long-term profiling of aerosol light extinction, particle mass, cloud condensation nuclei, and ice-nucleating particle concentration over Dushanbe, Tajikistan, in Central Asia. *Atmos. Chem. Phys.* **2020**, *20*, 4695–4711. [CrossRef]
27. Floutsi, A.A.; Korras-Carraca, M.; Matsoukas, C.; Biskos, G. The regime of aerosol optical depth over Central Asia based on MODIS Aqua Deep Blue data. In Proceedings of the EGU General Assembly Conference, Vienna, Austria, 12–17 April 2015; p. 13428.
28. Micklin, P. The Aral Sea disaster. *Annu. Rev. Earth Planet. Sci.* **2007**, *35*, 47–72. [CrossRef]
29. Chen, B.B.; Sverdlik, L.G.; Imashev, S.A.; Solomon, P.A.; Lantz, J.; Schauer, J.J.; Shafer, M.M.; Artamonova, M.S.; Carmichael, G. Empirical relationship between particulate matter and aerosol optical depth over Northern Tien-shan, Central Asia. *Air Qual. Atmos. Health* **2013**, *6*, 385–396. [CrossRef]
30. Ma, X.; Ding, Y.; Shi, H.; Yan, W.; Dou, X.; Ochege, F.U.; Luo, G.; Zhao, C. Spatiotemporal variations in aerosol optical depth and associated risks for populations in the arid region of Central Asia. *Sci. Total Environ.* **2021**, *816*, 151558. [CrossRef] [PubMed]
31. Ivanov, Y.N.; Chub, V.E.; Subbotina, O.I.; Tolkacheva, G.A.; Toryannikova, R.V. Review of the scientific and environmental issues of the Aral Sea basin. In *The Aral Sea Basin*; Springer: Berlin/Heidelberg, Germany, 1996; pp. 9–21. [CrossRef]
32. Hofer, J.; Althausen, D.; Abdullaev, S.F.; Nazarov, B.I.; Makhmudov, A.N.; Baars, H.; Engelmann, R.; Ansmann, A. Aerosol layer heights above Tajikistan during the CADEX campaign. *E3S Web Conf.* **2019**, *99*, 2009. [CrossRef]
33. Wang, D.; Zhang, F.; Yang, S.; Xia, N.; Ariken, M. Exploring the spatial-temporal characteristics of the aerosol optical depth (AOD) in Central Asia based on the moderate resolution imaging spectroradiometer (MODIS). *Environ. Monit. Assess.* **2020**, *192*, 383. [CrossRef] [PubMed]
34. Levy, R.C.; Mattoo, S.; Munchak, L.A.; Remer, L.A.; Sayer, A.M.; Patadia, F.; Hsu, N.C. The Collection 6 MODIS aerosol products over land and ocean. *Atmos. Meas. Tech.* **2013**, *6*, 2989–3034. [CrossRef]
35. Sayer, A.M.; Munchak, L.A.; Hsu, N.C.; Levy, R.C.; Bettenhausen, C.; Jeong, M.-J. MODIS Collection 6 aerosol products: Comparison between Aqua's e-Deep Blue, Dark Target, and "merged" data sets, and usage recommendations. *J. Geophys. Res. Atmos.* **2014**, *119*, 13965–13989. [CrossRef]
36. Superczynski, S.D.; Kondragunta, S.; Lyapustin, A.I. Evaluation of the multi-angleimplementation of atmospheric correction (MAIAC) aerosol algorithm through intercomparison with VIIRS aerosol products and AERONET. *J. Geophys. Res. Atmos.* **2017**, *122*, 3005–3022. [CrossRef]
37. Gelaro, R.; McCarty, W.; Suárez, M.J.; Todling, R.; Molod, A.; Takacs, L.; Randles, C.A.; Darmenov, A.; Bosilovich, M.G.; Reichle, R.; et al. The Modern-Era Retrospective Analysis for Research and Applications, Version 2 (MERRA-2). *J. Clim.* **2017**, *30*, 5419–5454. [CrossRef]
38. Rienecker, M.M.; Suarez, M.J.; Gelaro, R.; Todling, R.; Bacmeister, J.; Liu, E.; Bosilovich, M.G.; Schubert, S.D.; Takacs, L.; Kim, G.-K.; et al. MERRA: NASA's modern-era retrospective analysis for research and applications. *J. Clim.* **2011**, *24*, 3624–3648. [CrossRef]
39. Buchard, V.; Randles, C.A.; da Silva, A.M.; Darmenov, A.; Colarco, P.R.; Govindaraju, R.; Ferrare, R.; Hair, J.; Beyersdorf, A.J.; Ziemba, L.D.; et al. The MERRA-2 aerosol reanalysis, 1980 onward. Part II: Evaluation and case studies. *J. Clim.* **2017**, *30*, 6851–6872. [CrossRef]
40. Che, H.; Gui, K.; Xia, X.; Wang, Y.; Holben, B.N.; Goloub, P.; Cuevas-Agullo, E.; Wang, H.; Zheng, Y.; Zhao, H.; et al. Large contribution of meteorological factors to inter-decadal changes in regional aerosol optical depth. *Atmos. Chem. Phys.* **2019**, *19*, 10497–10523. [CrossRef]
41. Cao, S.; Zhang, S.; Gao, C.; Yan, Y.; Bao, J.; Su, L.; Liu, M.; Peng, N.; Liu, M. A long-term analysis of atmospheric black carbon MERRA-2 concentration over China during 1980–2019. *Atmos. Environ.* **2021**, *264*, 118662. [CrossRef]
42. Holben, B.N.; Eck, T.F.; Slutsker, I.; Tanré, D.; Buis, J.P.; Setzer, A.; Vermote, E.; Reagan, J.A.; Kaufman, Y.J.; Nakajima, T.; et al. AERONET—A federated instrument network and data archive for aerosolcharacterization. *Remote Sens. Environ.* **1998**, *66*, 1–16. [CrossRef]
43. Wang, J.; Li, X.; Christakos, G.; Liao, Y.; Zhang, T.; Gu, X.; Zheng, X. Geographical detectors-based health risk assessment and its application in the neural tube defects study of the Heshun region, China. *Int. J. Geogr. Inf. Sci.* **2010**, *24*, 107–127. [CrossRef]
44. Meng, X.; Gao, X.; Lei, J.; Li, S. Development of a multiscale discretization method for the geographical detector model. *Int. J. Geogr. Inf. Sci.* **2021**, *35*, 1650–1675. [CrossRef]
45. Chen, X.-L.; Zhao, H.-M.; Li, P.-X.; Yin, Z.-Y. Remote sensing image-based analysis of the relationship between urban heat island and land use/cover changes. *RemoteSens. Environ.* **2006**, *104*, 133–146. [CrossRef]
46. Martins, V.S.; Lyapustin, A.; Carvalho, L.A.S.; Barbosa, C.C.F.; Novo, E.M.L.M. Validation of high-resolution MAIAC aerosol product over South America. *J. Geophys. Res. Atmos.* **2017**, *122*, 7537–7559. [CrossRef]
47. Zhang, Z.; Wu, W.; Fan, M.; Wei, J.; Tan, Y.; Wang, Q. Evaluation of MAIAC aerosol retrievals over China. *Atmos. Environ.* **2019**, *202*, 8–16. [CrossRef]
48. Levy, R.C.; Remer, L.A.; Kleidman, R.G.; Matto, S.; Ichoku, C.; Kahn, R.A.; Eck, T.F. Global evaluation of the Collection 5 MODIS dark-target aerosol products over land. *Atmos. Chem. Phys.* **2010**, *10*, 10399–10420. [CrossRef]
49. Kang, N.; Kumar, K.R.; Hu, K.; Yu, X.; Yin, Y. Long-term (2002–2014) evolutionand trend in Collection 5.1 Level-2 aerosol products derived from the MODIS andMISR sensors over the Chinese Yangtze River Delta. *Atmos. Res.* **2016**, *181*, 29–43. [CrossRef]

50. Xi, X.; Sokolik, I.N. Seasonal dynamics of threshold friction velocity and dust emission in Central Asia. *J. Geophys. Res. Atmos.* **2015**, *120*, 1536–1564. [CrossRef] [PubMed]
51. Jiang, Q.; Yang, X. Sedimentological and Geochemical Composition of Aeolian Sediments in the Taklamakan Desert: Implications for Provenance and Sediment Supply Mechanisms. *J. Geophys. Res. Earth Surf.* **2019**, *124*, 1217–1237. [CrossRef]
52. Han, T.; Pan, X.; Wang, X. Evaluating and improving the sand storm numerical simulation performance in Northwestern China using WRF-Chem and remote sensing soil moisture data. *Atmos. Res.* **2021**, *251*, 105411. [CrossRef]
53. Xi, X.; Sokolik, I.N. Dust interannual variability and trend in Central Asia from 2000 to 2014 and their climatic linkages. *J. Geophys. Res. Atmos.* **2015**, *120*, 12–75. [CrossRef]
54. Sokolik, I.N.; Darmenova, K.; Huang, J.; Kalashnikova, O.; Kurosaki, Y.; Xi, X. Examining changes in land cover and land use, regional climate and dust in dryland East Asia and their linkages within the Earth system. In *Dryland East Asia (DEA): Land Dynamics Amid Social and Climate Change*; Chen, J., Wan, S., Henebry, G., Qi, J., Gutman, G., Sun, G., Kappas, M., Eds.; DE GRUYTER: Berlin, Germany, 2013; pp. 185–213.
55. Orlovsky, N.; Orlovsky, L. White sand storms in Central Asia. In *Global Alarm: Dust and Sand Storms from the World's Drylands*; Yang, Y., Squires, V., Lu, Q., Eds.; UNCCD: Bangkok, Thailand, 2002; pp. 169–201.
56. De Meij, A.; Bossioli, E.; Penard, C.; Vinuesa, J.F.; Price, I. The effect of SRTM and Corine Land Cover data on calculated gas and PM10 concentrations in WRF-Chem. *Atmos. Environ.* **2015**, *101*, 177–193. [CrossRef]
57. Ginoux, P.; Prospero, J.M.; Gill, T.E.; Hsu, N.C.; Zhao, M. Global-scale attribution of anthropogenic and natural dust sources and their emission rates based on MODIS Deep Blue aerosol products. *Rev. Geophys.* **2012**, *50*, RG3005. [CrossRef]
58. Yang, X. Desertification and land use in arid areas of Central Asia. *Quat. Res.* **1998**, *2*, 119–127.
59. Zhang, F.; Yushanjiang, A.; Jing, Y. Assessing and predicting changes of the ecosystem service values based on land use/cover change in Ebinur Lake Wetland National Nature Reserve, Xinjiang, China. *Sci. Total Environ.* **2019**, *656*, 1133–1144. [CrossRef]
60. Zeng, H.; Wu, B.; Zhu, W.; Zhang, N. A trade-off method between environment restoration and human water consumption: A case study in Ebinur Lake. *J. Clean. Prod.* **2019**, *217*, 732–741. [CrossRef]
61. Gao, W.; Yuan, Y.; Liu, Z.; Wei, W. Analysis of dust sources and dust aerosol release conditions in Xinjiang. *China Desert* **2008**, *5*, 968–973.
62. Jugder, D.; Shinoda, M.; Sugimoto, N.; Matsui, I.; Nishikawa, M.; Park, S.-U.; Chun, Y.-S.; Park, M.-S. Spatial and temporal variations of dust concentrations in the Gobi Desert of Mongolia. *Glob. Planet. Chang.* **2011**, *78*, 14–22. [CrossRef]
63. Meng, X.; Gao, X.; Li, S.; Li, S.; Lei, J. Monitoring desertification in Mongolia based on Landsat images and Google Earth Engine from 1990 to 2020. *Ecol. Indic.* **2021**, *129*, 107908. [CrossRef]
64. Li, C.; Zhang, Y.; Liu, Z.; Wang, R. Response of desertification to climate change and Control Countermeasures in Xinjiang. *Bull. Soil Water Conserv.* **2014**, *34*, 264–268. [CrossRef]
65. Chi, M. Remote Sensing Analysis of Land Use Types in Dust Source Areas of East Asia. Master's Thesis, Inner Mongolia Normal University, Hohhot, China, 2020. [CrossRef]
66. Alizade Govarchin Ghale, Y.; Tayanc, M.; Unal, A. Dried bottom of Urmia Lake as a new source of dust in the northwestern Iran: Understanding the impacts on local and regional air quality. *Atmos. Environ.* **2021**, *262*, 118635. [CrossRef]
67. Arkian, F.; Nicholson, S.E. Long-term variations of aerosol optical depth and aerosol radiative forcing over Iran based on satellite and AERONET data. *Environ. Monit. Assess.* **2018**, *190*, 1. [CrossRef]
68. Chen, W.; Ding, J.; Tan, J.; Zhang, J.; Liu, B. Analysis of desertification change in Central Asia from 2000 to 2015 based on DPM-SPOT. *Geogr. Arid Areas* **2018**, *41*, 119–126. [CrossRef]